Article

Fabrication and In Vitro Evaluation of LL37-Loaded Electrospun PHB/Collagen Nanofibers for Wound Healing

Beyza Nur Sayaner Taşçı *, Sümeyye Kozan, Meltem Demirel Kars, Kemal Çetin, Sema Karslıoğlu, Gökhan Kars *

Posted Date: 6 August 2025

doi: 10.20944/preprints202508.0224.v1

Keywords: biofiber; collagen; LL37; PHB; wound healing

 doi:10.20944/preprints202508.0224.v1

Article

Fabrication and In Vitro Evaluation of LL37-Loaded Electrospun PHB/Collagen Nanofibers for Wound Healing

Beyza Nur Sayaner Taşçı [1, *], Sümeyye Kozan [2], Meltem Demirel Kars [2], Kemal Çetin [2], Sema Karslıoğlu [3] and Gökhan Kars [1, *]

[1] Department of Molecular Biology and Genetics, Faculty of Science, Necmettin Erbakan University, Konya 42140, Türkiye

[2] Department of Biomedical Engineering, Faculty of Engineering, Necmettin Erbakan University, Konya 42140, Türkiye

[3] Department of Basic Sciences, Faculty of Engineering, Necmettin Erbakan University, Konya 42140, Türkiye

* Correspondence: 22820511006@erbakan.edu.tr (B.N.S.T.); gkars@erbakan.edu.tr (G.K.)

Abstract

Skin repair is essential in the treatment of burns and wounds. After an injury, the concept of tissue engineering emerges to restore skin function and facilitate wound healing. This field often involves the use of biodegradable and biocompatible materials as a primary scaffold for tissue regeneration. In this study, a PHB/Collagen wound dressing mat loaded with the antimicrobial peptide LL37 was developed via electrospinning. The polymer solutions were prepared by dissolving polyhydroxybutyrate (PHB) biopolymer extracted from *Cereibacter sphaeroides*, commercial PHB, and marine collagen in hexafluoroisopropanol (HFIP). The resulting nanofibers were characterized using Field-Emission Scanning Electron Microscopy (FE-SEM), Thermogravimetric Analysis (TGA), X-Ray Diffractometry (XRD), and an Optical Tensiometer. Antibacterial activity assessments were conducted against *Staphylococcus aureus* (ATCC 29213) and *Escherichia coli* (ATCC 25922). Degradability studies were carried out in DMEM medium, cytotoxicity tests were performed on the L929 fibroblast cell line, and the wound healing effect was investigated on the HS2 keratinocyte cell line. To evaluate the properties of the designed material under in vitro conditions, the morphology of cells on the nanofiber was examined using an inverted light microscope. The findings demonstrated that the nanofibers were biocompatible *in vitro* and exhibited no toxic effects. And, compared to the control groups, the 5.57 µM LL37-loaded PHB/Collagen nanofibers significantly enhanced wound closure by 15–30% and effectively reduced the viability of *S. aureus* and *E. coli* by 20–25% and approximately 80–85%, respectively. These results highlight the therapeutic potential of LL37-loaded PHB/Collagen nanofibers for use in wound healing applications.

Keywords: biofiber; collagen; LL37; PHB; wound healing

1. Introduction

Polymers are high-molecular-weight macromolecules formed by the association of repeating monomer units with covalent bonds. Based on their sources and biological properties, they are classified as natural polymers (e.g., polysaccharides and proteins), biodegradable synthetic polymers (esters, amides, ethers, urethanes), and hybrid systems [1]. Biopolymers, among these groups, are noteworthy materials in biomedical applications due to their natural origin, biodegradable structure, and biocompatible properties. Biopolymers are generally divided into three main categories: (i)

 doi:10.20944/preprints202508.0224.v1

biopolymers obtained from agricultural sources such as starch, (ii) polymers such as polyhydroxyalkanoates (PHA) obtained through microbial activities, and (iii) polymers such as polylactic acid (PLA) synthesized through biotechnological means [2].

Wound healing is a clinically important process, particularly in the treatment of chronic wounds and burns. Such wounds increase the risk of infection, prolong the healing process, and pose a significant economic burden on healthcare systems [3]. Therefore, the need for biomaterial systems that accelerate wound healing, prevent infections, and support tissue repair is increasing. Tissue engineering is gaining prominence in this context, and structures that support cell growth are being developed using biodegradable and biocompatible scaffolding materials [4].

Collagen, one of the natural polymers, is the most abundant structural protein in the extracellular matrix. Its advantages, such as low antigenicity, biocompatibility, and biodegradability, make it widely used in wound dressings. Collagen supports fibroblast proliferation, promotes endothelial cell migration, stimulates coagulation, and contributes to scar formation [3]. These properties make collagen a frequently preferred natural biopolymer in wound healing. Furthermore, polyhydroxybutyrate (PHB), a microbially derived biopolymer, is a member of the PHA family and has also biodegradable and biocompatible structures. Its potential for natural interaction with human blood and tissues makes it an attractive material for biomedical applications [5]. PHB synthesis generally occurs through the metabolism of carbon sources such as glucose by microorganisms. Bacteria such *as Bacillus, Pseudomonas, Klebsiella, Streptomyces, Mycobacterium, Rhodococcus,* and *Escherichia* play a significant role in PHB production [6].

Today, the development of antimicrobial biomaterials to prevent wound infections is attracting considerable interest. Antimicrobial peptides (AMPs) exhibit broad-spectrum antimicrobial activity by strongly interacting with bacterial cell membranes due to their positively charged and hydrophobic structures [7]. These peptides, which can be physically or chemically immobilized on nanofiber surfaces, have the potential to replace traditional antibiotics [8]. One of these peptides, LL37, is a positively charged molecule with an α-helical structure and exhibits strong antibacterial activity under physiological conditions such as pH 6. LL37 provides antimicrobial activity by disrupting the integrity of the bacterial membrane. However, it also has limitations such as low biological stability, sensitivity to proteolytic enzymes, and potential cytotoxicity [7].

In this study, multifunctional biocompatible and antibacterial wound dressing mats were designed by integrating the LL37 peptide into an electrospun biofiber mat containing commercial and bacterial PHB and collagen. The structural characterization, antibacterial activity, and cellular biocompatibility of the developed system were thoroughly evaluated in vitro. The findings demonstrate the potential of this next-generation biomaterial platform for wound healing.

2. Materials and Methods

2.1. Chemicals and Materials

PHB extracted from *Cereibacter sphaeroides* O.U.001, commercially available PHB (500 kDa, Merck, Darmstadt, Germany), marine-derived collagen, LL37 antimicrobial peptide (QYABIO, Sigma-Aldrich, St. Louis, MO, USA), 1,1,1,3,3,3-Hexafluoro-2-propanol (HFIP) (Abcr, Karlsruhe, Germany), Dulbecco's Modified Eagle Medium (DMEM) (Gibco, Grand Island, NY, USA), fetal bovine serum (FBS), gentamicin (Sigma-Aldrich, St. Louis, MO, USA), and XTT (3-(4,5-dimethylthiazol-2-yl)-2,5-diphenyltetrazolium bromide assay, Sartorius, Göttingen, Germany) were purchased.

2.2. Method

2.2.1. Development of LL37-loaded PHB/Col Nanofiber Mats

Bacterial PHB, commercial PHB and marine-collagen were utilized as the polymeric components. Bacterial PHB was incorporated at varying percentages of the total PHB content, i.e.,

 doi:10.20944/preprints202508.0224.v1

0%, 25%, 50%, 75%, and 100% (w/w). Nanofibers were prepared according to previously described method with some modifications [9]. For each formulation, 20 mL of polymer solutions were prepared, maintaining a total polymer concentration of 2% (w/v) with a PHB/collagen ratio of 1:1 (w/w) (Table 1). These solutions were sonicated using a Bandelin Sonopuls HD 2200 MS 72 (Bandelin Electronic, Berlin, Germany) in an icebox for 10 min and homogenized by overnight stirring using a magnetic stirrer to ensure complete dissolution and uniform dispersion. The prepared polymer solutions were transferred into 10 mL syringes and electrospun onto aluminum foil collectors using a syringe pump. Optimized electrospinning parameters (a flow rate of 1.8 mL/h, a working distance of 18 cm, and an applied voltage of 27 kV) were employed to produce nanofiber wound dressing prototypes. The PHB/Collagen nanofibers were loaded with the antimicrobial peptide LL37 via a physical adsorption method. Specifically, 25 µL of LL37 solution (1 mg/mL) was precisely dripped onto circular nanofiber samples (0.6 cm in diameter) and allowed air dry (Figure 1).

Table 1. The parameters for the nanofiber manufacture process.

Nanofiber types	$PHB_{(b)}^{*}/PHB_{(c)}^{**}$ (w/w)	Collagen (w)	Solvent
NF-1 : %0 bacterial PHB/Collagen	0 g $PHB_{(b)}$ / 0.2 g $PHB_{(c)}$	0.2 g	HFIP
NF-2 : %25 bacterial PHB/Collagen	0.05 g $PHB_{(b)}$ / 0.15 g $PHB_{(c)}$	0.2 g	HFIP
NF-3 : %50 bacterial PHB/Collagen	0.1 g $PHB_{(b)}$ / 0.1 g $PHB_{(c)}$	0.2 g	HFIP
NF-4 : %75 bacterial PHB/Collagen	0.15 g $PHB_{(b)}$ / 0.05 g $PHB_{(c)}$	0.2 g	HFIP
NF-5: %100 bacterial PHB/Collagen	0.2 g $PHB_{(b)}$ / 0 g $PHB_{(c)}$	0.2 g	HFIP

*$PHB_{(bacterial)}$, **$PHB_{(commercial)}$

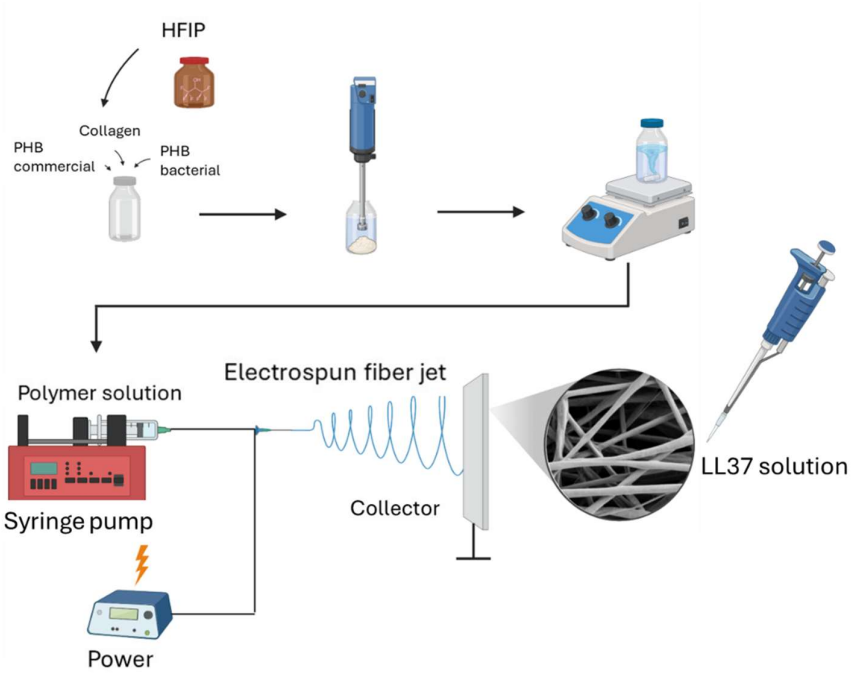

Figure 1. Schematic representation of PHB/Col/LL37 nanofibers.

2.2.2. Physicochemical Characterization of LL37/PHB/Col Nanofiber Mats

The morphological characteristics of PHB/Collagen nanofiber mats were analyzed using a field-emission scanning electron microscope (FE-SEM) (Gemini SEM 500, Zeiss, Oberkochen, Germany). The samples were examined under an accelerating voltage of 2 kV to ensure high-resolution imaging. The fiber diameters were measured and analyzed by image J program and the fiber diameters were presented on histogram graphs. The wettabilities of the nanofiber mats were tested by digital video-

 doi:10.20944/preprints202508.0224.v1

based optical contact angle measurement using a Biolin Scientific Attension Theta Lite instrument (Biolin Scientific, Göteborg, Sweden.)

The chemical characterization was performed by common methods; FT-IR, XRD, and Thermal-gravimetric analyses. FT-IR analysis was used to identify specific functional groups present in the chemical bonds of fiber materials; X-ray diffraction (XRD) analysis was conducted to reveal the distribution and crystalline structure of the nanofibers; and thermogravimetric analysis (TGA, Setaram, Labsys Evo, Caluire, France) was performed to determine the mass loss of the nanofibers in response to temperature changes.

2.2.3. Degradation of Nanofibers

In vitro degradability testing of PHB/Collagen wound dressing functionalized with LL37 antimicrobial peptide was carried out to obtain information about the durability, efficacy and safety of the nanofiber material. In this context, NF-1, NF-2 and NF-3 were cut into 0.6 cm diameter disks with the help of a punch. The discs were placed in 96-well microplates in triplicate and 150 µL DMEM medium was added to each well. Nanofiber discs were removed from the medium on days 1, 7 and 14, dried and weighed. Based on the data, % weight loss of the samples was calculated and degradability profile of nanofibers was evaluated.

2.2.4. In Vitro Biocompatibility and Cell Attachment on Nanofibers

The *in vitro* biocompatibility of PHB/Collagen NF wound dressing samples was assessed by evaluating their effects on the proliferation of mouse fibroblast L929 cells. NFs were incubated in blank medium (L929, DMEM) for 24, 48 and 72 h. At the end of these periods, nanofibers were removed from the medium which will be tested for biocompatibility. Then, 5×10^3 L929 cells per well were added to each well of the 96-well microplate, except for the negative control and medium control, and the cells were incubated for 24 h for attachment. At the end of the incubation period, the medium was removed, and the nanofiber extracts were transferred to the wells. The extract-treated cells were visualized with an inverted light microscope (10X magnification), then 50 µL of XTT solution was added to each well. After incubating the plate for 4 h, optical density (OD) values were measured using a microplate spectrophotometer at 450 nm. The data was used to evaluate the effect of nanofibers on cell viability. The cell viability percentage of L929 cells was calculated using Equation 1.

$$\text{Cell viability (\%)} = \frac{\text{The optical density (OD) of the sample 450nm}}{\text{The OD of the positive control} - \text{The OD of the negative control 450}} \times 100 \qquad \text{Equation 1}$$

The biocompatibility of the LL37 AMP-loaded PHB/Collagen nanofiber wound dressing mats and cell attachment ability on NF1-NF3 were analyzed by confocal laser scanning microscope (CLSM) (Zeiss, Oberkochen, Germany) and scanning electron microscopy (SEM, Hitachi High-Tech Corp., Tokyo, Japan) to evaluate cell adhesion.

The nanofibers were punched into 0.6 cm diameter discs and sterilized on both sides under UV light for 30 min. They were then placed into 96-well cell culture plates and rinsed twice with PBS. Keratinocytes cells were seeded at 1.5×10^5 cell density in DMEM medium (supplemented with 70% FBS and gentamicin) onto each nanofiber scaffold. After allowing the cells to adhere to the nanofiber surface, the samples were rinsed with 0.1 M sodium cacodylate buffer (pH 7.4) and fixed by immersion in 3% glutaraldehyde. For confocal microscopy after fixation, fibers were rinsed with 300 µL of Tween-80 solution and the fibers were treated with Triton-X solution for 5 min. The staining solution (rhodamine-phalloidin and DAPI) was applied to the fibers, followed by incubation for 20 min. Subsequently, the samples were washed with Tween-80 and then prepared for confocal microscopy by adding 1 mL of PBS. For SEM analysis, following fixation, the samples were washed with distilled water and dehydrated in ethanol solutions (50%, 75%, 90%, and 100% v/v). The dehydrated samples were then treated with HMDS and dried overnight in a fume hood. Finally, the samples were coated with iridium and analyzed under SEM.

 doi:10.20944/preprints202508.0224.v1

2.2.5. Measurement of 2D Wound Healing Activity by Scratch Assay

The *in vitro* wound healing effects of the NF-1-3/LL37 were evaluated using the scratch assay technique. In this study, 0.4×10^5 human keratinocyte cells were seeded into each well of a 96-well microplate and incubated to allow the cells to cover the surface. A scratch was made in each well using a sterile 100 µL pipette tip. The microplate was divided into two groups with three replicates each: NF1-3/LL37 and blank NF1-3 and the corresponding nanofiber samples were placed over the scratches. On days 1, 3, and 7, the nanofibers were removed, and the scratch closure was observed under an inverted light microscope (4X magnification). The images were analyzed using ImageJ software to measure the scratch closure rates and evaluate the wound healing potential. The scratch closure percentage was calculated according to Equation 2, where A_0 is initial scratch width and A_t is scratch width at a given time.

$$\text{Scratch closure (\%)} = \frac{A0-At}{A0} \times 100 \qquad \text{Equation 2}$$

2.2.6. Evaluation of Antibacterial Activity of Nanofiber Mats

The *in vitro* antibacterial activity of NF mats was evaluated against *Escherichia coli* (ATCC 25922) and *Staphylococcus aureus* (ATCC 29213). For this purpose, bacterial strains were cultured on Mueller Hinton Agar (MHA) at 37 °C for 16 h. Nanofiber discs with a diameter of 0.6 cm were sterilized under UV light, after which 25 µL of LL37 solution (1 mg/mL) was dropped onto each disc and left to dry under sterile conditions. Bacterial suspensions were adjusted to the 0.5 McFarland standard. Each well received 90 µL of Mueller Hinton Broth (MHB), and 10 µL of the prepared bacterial suspension was added to the wells and nanofiber discs NF-1-NF-3/LL37 were placed on bacteria suspension, in triplicate. For the negative control group, Gentamicin and Oxacillin antibiotic discs were placed into the wells. The non-treated bacteria suspension was served as positive control for cell viability. The plate was incubated at 37 °C for 16 h. After incubation, optical density (OD) measurements at 600 nm were performed using a 96 well plates reader to assess antibacterial activity. These measurements were used to determine the inhibitory effects of the nanofibers on bacterial growth.

3. Results and Discussion

3.1. Physicochemical Characteristics of PHB/Col/LL37 Nanofiber Mats

The elecrtospun nanofibers were manufactured with different PHB/Collagen ratios were tested by Salvatore et al. and it was found that increasing the collagen content (1:1 ratio) affected both viscosity and fiber diameter due to increased solution viscosity [9]. Similarly, Prabhakaran et al. reported the inverse effect of collagen content on fiber size in PHBV/Collagen blends. Accordingly, a PHB/Collagen ratio of 1:1 was adopted in this study [10]. Among the six different PHB_b: PHB_c containing polymer slurries, the ones containing 0%, 25%, and 50% bacterial PHB were resulted in successfully spun nanofibers (Figure 2). Nanofiber formation was not observed with 75% and 100% PHB_b/Collagen solutions (NF-4 and NF-5). This may be because of the very low dissolution of bacterial PHB at higher ratios which may be stemmed from low molecular weight PHB_b, resulting in a turbid, low-viscosity solution

 doi:10.20944/preprints202508.0224.v1

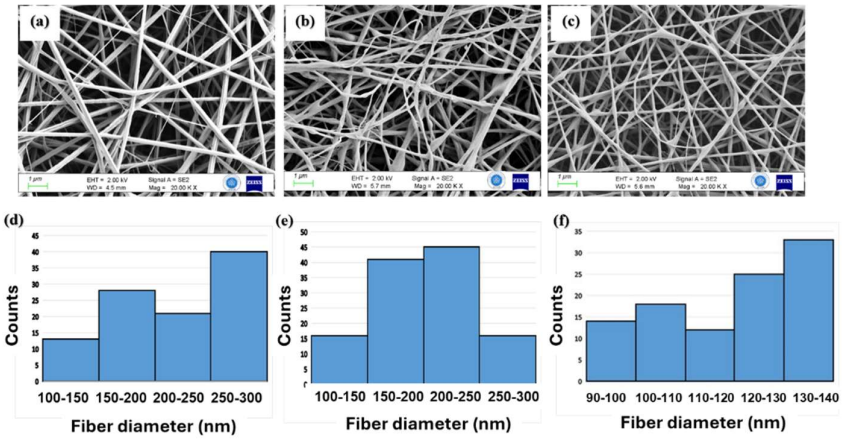

Figure 2. FE-SEM images of PHB/Col nanofibers and distribution of fiber diameters (a,) (d) NF-1, (b), (e) NF-2 and (c),(f) NF-3.

Detailed FE-SEM analysis at 20.00 KX magnification revealed a uniform, bead-free network structure of the nanofibers. Further analysis using ImageJ enabled estimation of average fiber diameter and distribution for each membrane type. It is well known that viscosity significantly affects jet formation and fiber thinning during electrospinning. Lower viscosity typically yields finer fibers. In this study, increasing the bacterial PHB content reduced solution viscosity, resulting in more uniform and thinner fibers. Mean fiber diameters of NF-1, NF-2 anf NF-3 were found to be 232,80 ± 62.04 nm, 212.64 ± 53.73 nm and 119.82 ± 18.25 nm respectively (Figure 2). The LL37 loaded nanofibers were presented by FE-SEM analysis as a supplementary figure (Figure S1).

FT-IR analysis was performed to identify the functional groups of PHB extracted from *Cereibacter sphaeroides*, as well as commercial PHB and collagen obtained from Sigma Aldrich. Functional groups of PHB were examined by comparing characteristic peaks at specific wavelengths. The FT-IR spectra of bacterial and commercial PHB, along with marine collagen, were recorded between 4000 and 500 cm^{-1} (Figure 3), and corresponding functional groups are listed in Table 2.

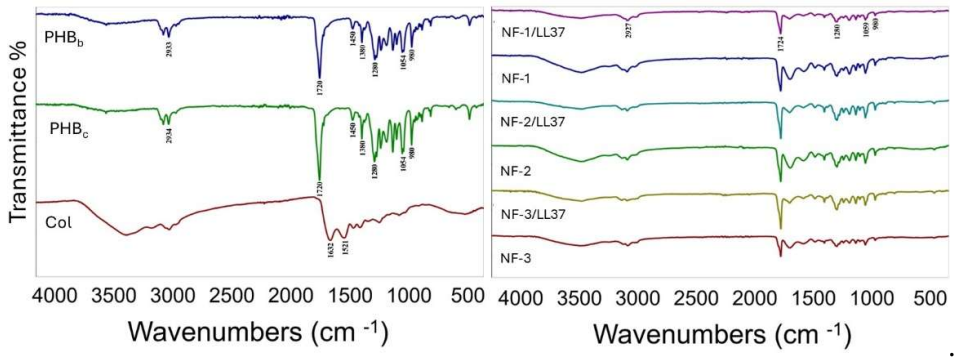

Figure 3. FT-IR spectra of raw materials of polymer slurry (PHBc, PHBb, Col) and that of NF mats.

The FT-IR spectrum of PHB showed characteristic peaks confirming the presence of polyhydroxybutyrate in the nanofibers. As expected, the polymer exhibited a strong C=O peak, verifying its identity as PHB [11]. As shown in Table 2 and Figure 3, absorption at 2976–2932 cm^{-1} indicated aliphatic CH streching, while the peak at 1724–1719 cm^{-1} corresponded to the C=O stretching vibration of ester groups. Additional peaks at 1453 cm^{-1} (CH_2 scissoring), 1380 cm^{-1} (CH_3 bending), and 1275–1280 cm^{-1} (C–O stretching) further confirmed the structure. In line with Prabhakaran et al., collagen-specific amide I and II peaks were observed at 1632 cm^{-1} and 1521 cm^{-1}, validating the presence of marine-derived collagen in the NF samples [10].

 doi:10.20944/preprints202508.0224.v1

Table 2. Functional groups of FT-IR spectra.

Functional group	Wavenumbers (cm^{-1})
CH_3	1380
CH_2	1450
C-H	2976-2932
C=O	1724-1719
C-O	1280-1275
O-H	3436

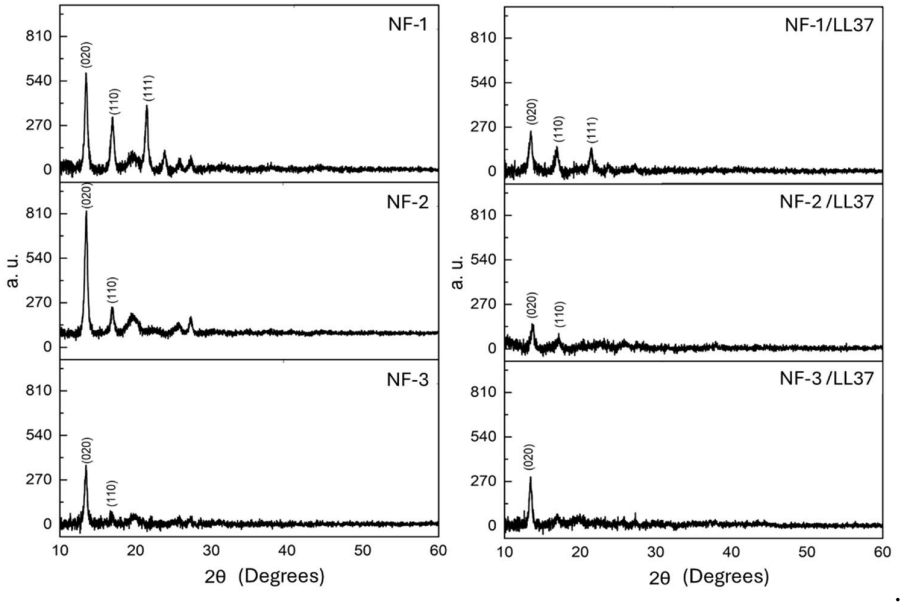

Figure 4. XRD spectra of NFs.

X-ray diffraction (XRD) patterns in Figure 4 compare the crystalline characteristics of three samples containing 50% collagen and varying PHB content. Distinct diffraction peaks corresponding to PHB's orthorhombic crystal planes (020), (110), and (111) are observed near 2θ ≈ 13°, 17°, and 22° in all samples. The sample with 0% PHB_b (NF-1), containing only commercial PHB (≈500 kDa), exhibits the most intense and sharp peaks, indicating high crystallinity due to its regular and ordered chain packing.. In the sample with 25% PHB_b (NF-2) (≈102 kDa), peak intensities decrease and broaden, suggesting limited crystal formation due to lower molecular weight and decreased chain regularity. With 50% PHB_b (NF-3), peak intensity, especially for the (111) plane, decreases markedly, indicating a substantial reduction in crystallinity. The presence of low-molecular-weight bacterial PHB and amorphous collagen disrupts ordered crystal formation. The diffractograms also show XRD results after incorporation of antimicrobial peptide LL37. LL37 further reduces PHB crystallinity, evident from weakened and broadened peaks. While characteristic reflections persist in the NF-1/LL37 sample, crystallinity continues to decline in NF-2/LL37 and NF-3/LL37 samples, with some peaks disappearing entirely. These results indicate that LL37 physically disrupts the polymer crystalline domains. Due to its amphiphilic nature and low molecular weight (4493 Da), LL37 diffuses between PHB chains, weakening secondary bonds and hindering chain interactions, thereby suppressing crystal formation. This behavior resembles classical plasticizer mechanisms. The low molecular weight and irregular structure of bacterial PHB further facilitate LL37's interference with chain packing. Increased PHB_b content combined with LL37 addition reduces crystallinity and enhances polymer chain mobility, enabling the production of finer nanofibers through easier fiber spinning.

 doi:10.20944/preprints202508.0224.v1

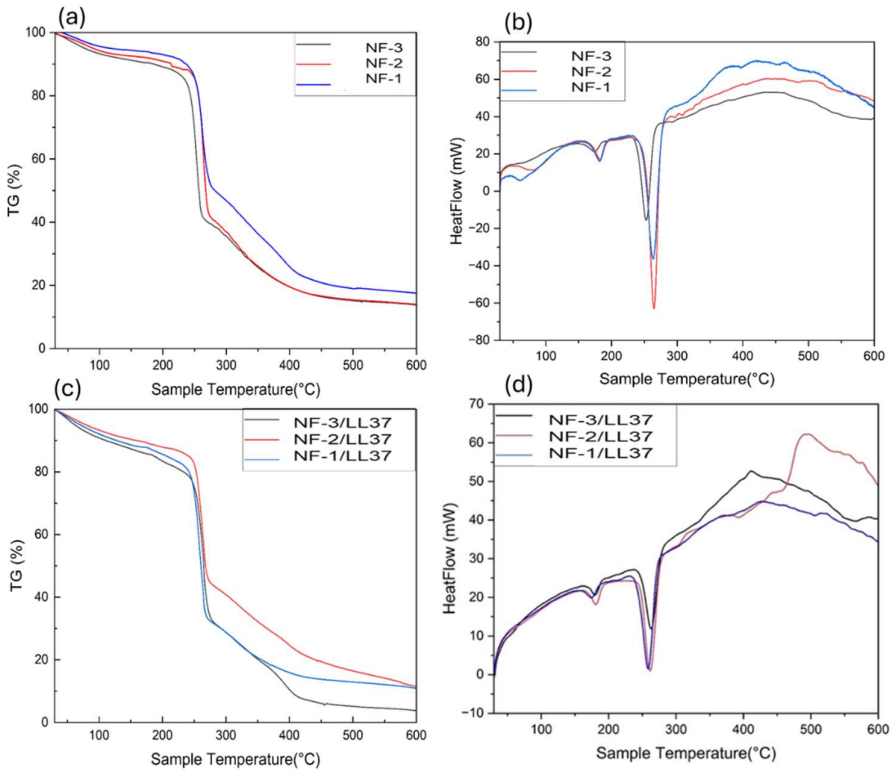

Figure 5. Thermal properties of PHB/Collagen samples containing LL37 and varying ratios of bacterial PHB (PHB_b). (a), (c) Thermogravimetric analysis (TGA) curves, (b), (d) Differential scanning calorimetry (DSC) curves.

According to TGA results, all samples show primary degradation between 280–310 °C, with degradation profiles varying based on PHB_b content. The earliest degradation is observed in the sample NF-3, which contains the highest proportion of low-molecular-weight PHB_b followed by NF-2 and NF-3 samples. This is attributed to the the reduced chain length and structural disorder of PHB_b, which increases susceptibility to thermal decomposition. In contrast, the NF-1, containing only PHB_c, shows delayed degradation and greater thermal stability due to its higher molecular weight and crystallinity. Residue analysis shows the highest char yield in the NF-1, with decreasing residues as PHB_b content increases. This suggests that bacterial PHB disrupts the crystalline structure, accelerates degradation, and limits carbonization due to the volatility of its short-chain decomposition products.

DSC data support these findings. All samples exhibit PHB related melting peaks around 175–180 °C, but peak intensity decreases with higher PHB_b content. NF-1 shows a sharp, high-enthalpy peak, indicating high crystallinity, while NF-2 and NF-3 samples show broader, weaker peaks, reflecting disrupted crystal formation. Broad exothermic transitions between 300–500 °C are linked to collagen degradation and internal oxidation, and these transitions diminish with increasing PHB_b content.

Overall, higher bacterial PHB content reduces crystallinity and thermal stability, shifting the material toward a more amorphous structure. This is consistent with earlier onset of degradation in TGA and weaker melting peaks in DSC. While PHB_b enhances processability, it compromises crystallinity and thermal resistance. Figure 5 illustrates how LL37 and varying PHB_b ratios affect thermal behavior in PHB/collagen samples. TGA confirms degradation onset shifts earlier with increasing PHB_b, especially at 50%. Residual mass decreases significantly at high PHB_b content. DSC results show diminishing and broadening melting peaks with increased PHB_b, reflecting greater amorphous character. Broad exothermic transitions between 300–500 °C are primarily due to collagen

 doi:10.20944/preprints202508.0224.v1

pyrolysis, with the 25% PHBb sample showing the most pronounced response, possibly due to synergistic degradation of collagen and peptide interactions. In conclusion, increasing PHBb reduces crystallinity and thermal stability, and LL37 acts as a secondary plasticizing agent, disrupting chain packing and enhancing matrix degradation.

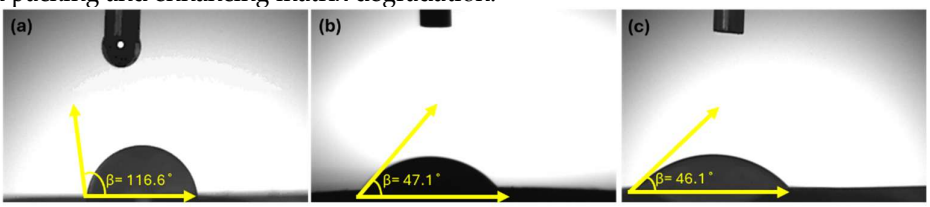

Figure 6. Average water contact angles of (a) NF-1/LL37, (b) NF-2 /LL37, (c) NF-3 /LL37 samples were measured as 116.6, 47.1 and 46.1 respectively.

In this study, nanofibers were produced by blending PHB extracted from *Cereibacter sphaeroides*, commercial PHB, and marine-derived collagen, and loaded with the antimicrobial peptide LL37. Figure 6 presents water contact angle (WCA) measurements used to assess the wettability of the developed nanofibrous scaffolds. The water contact angle (WCA) of the nanofiber with 0% bacterial PHB was 116.6°, indicating a hydrophobic surface. Increasing the bacterial PHB content to 25% and 50% reduced the WCA to 47.1° and 46.1°, respectively. These results demonstrate that higher bacterial PHB content significantly enhances hydrophilicity and improves the wettability of the nanofiber surface.

In a study, the water contact angle (WCA) of PHB nanofibrous scaffolds, which have a hydrophobic structure due to their crystalline regions, was measured as 91.49°. The water contact angle of PHB/CTS biocomposite nanofibrous scaffolds, fabricated by blending PHB with CTS, was measured as 44.39°, which is significantly lower than that of PHB. The hydrophilicity of CTS is primarily attributed to its hydrophilic amino and hydroxyl groups. As a result, when blended with PHB, CTS was observed to enhance the wettability of the fibrous scaffold [12]. The surface wettability of collagen nanofibers was investigated by Naderi Gharahgheshlagh et al. This test was performed on electrospun collagen nanofibers; however, due to the high hydrophilicity of this biopolymer, water droplets were rapidly absorbed, making it impossible to measure the water contact angle for the electrospun Kol-cotton, Kol/EPS1%-cotton, and Kol/EPS2%-cotton samples [13]. LL37 antimicrobial peptide, which possesses an α-helical structure, exhibit amphiphilic properties; one end of such peptides is hydrophilic, while the other end has a hydrophobic region. This hydrophilic and lipophilic structure forms the basis of the antimicrobial function of this peptide [14].

3.2. Degradation of Nanofibers

Weight loss results exhibited that the cumulative degradation % of all samples ranged between 30% and 50%. The weight losses for NF-1, NF-2 and NF-3 samples at the end of 14 days were approximately 30%, 15%, and 50%, respectively. When the weight loss results are compared, the highest weight loss was observed in the 50% PHBb/Collagen sample, while the lowest was observed in the 25% PHBb /Collagen sample. In a study conducted by Mohammadalipour et al., the biodegradability of PHB and PCL polymers was investigated, and it was reported that a reduction in fiber diameter and crystallinity in scaffolds resulted in enhanced surface contact and easier PBS penetration, leading to higher biodegradability [15]. Similarly, in this study, a progressive decrease in nanofiber diameter was observed in the 0%, 25%, and 50% bacterial PHB/Collagen nanofibers. Consequently, the bacterial PHB/Collagen nanofiber with 50% PHBb content, which had the smallest fiber diameter, exhibited the highest biodegradability.

3.4. Biocompatibility and Cell Attachment on Nanofibers

Fiber mats were incubated in cell culture medium for 24, 48, and 72 h. These extracts were then incubated with L929 cells previously seeded on culture plates for 24 and 48 h, and the cells were

 doi:10.20944/preprints202508.0224.v1

observed under an inverted microscope at 10X magnification. The effects of the extracts on cell proliferation were also evaluated after 48 h of incubation using the XTT cytotoxicity assay kit. Considering the proliferation of the control cell group as 100%, the proliferation rates of the cells incubated with the test groups were determined. As shown in Figure 7, cell proliferation values were found to be above 70%. Based on Figures S2-S4, and taking cell morphology into account, it was concluded that the fiber mat samples were biocompatible. Cell images are presented as supplementary documents.

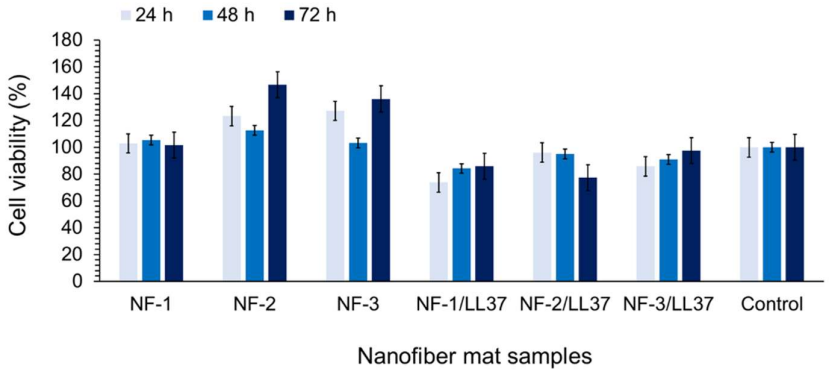

Figure 7. Effects of NF samples on cell proliferations after 24h, 48 h and 72 h treatment with NF sample extracts.

SEM and confocal microscopy images of the PHB/Collagen nanofibers revealed the cell adhesion profiles on the nanofiber surfaces and demonstrated that cell attachment occurred on the non-toxic PHB/Collagen/LL37 nanofibers. As shown in Figure 8 keratinocyte adhesion was observed on the nanofiber mats containing 0%, 25%, and 50% bacterial PHB/Collagen/LL37 which are NF-1/LL37, NF-2/LL37 and NF-3/LL37 respectively.

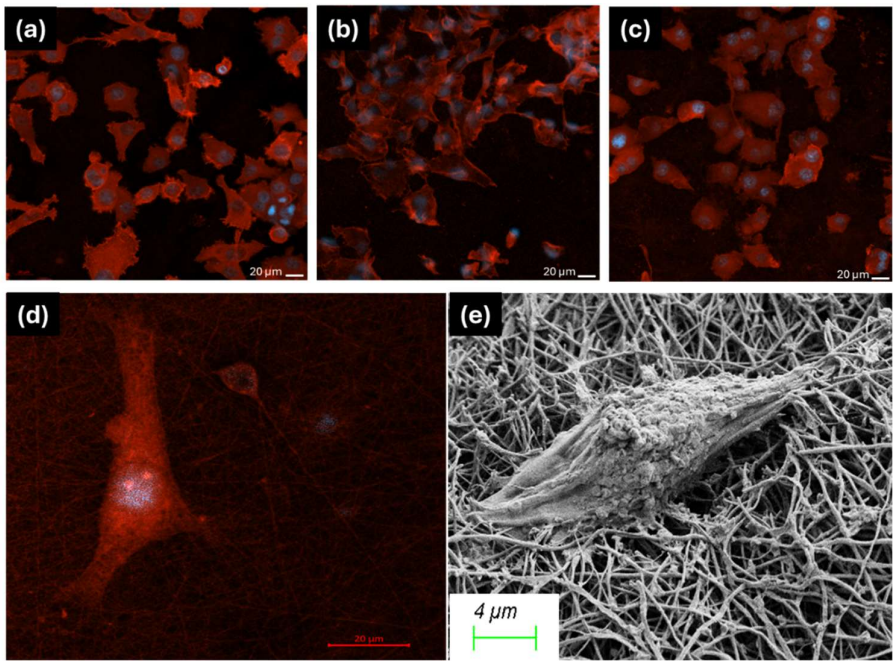

Figure 8. The CLSM images of keratinocyte cells attached to (a) NF-1/LL37, (b) NF-2/LL37, (c), (d) NF-3/LL37 samples. Nuclei were stained with DAPI (blue) and F-actin was stained using Rhodamine-phalloidin. The cell attachment to the fiber matrix was also demonstrated by SEM (e).

 doi:10.20944/preprints202508.0224.v1

3.5.2. D Wound Healing Activity of Nanofiber Mats

Wound closure percentages on days 1, 3, and 7 were calculated based on measurements from the microscopic images. Figure 9 shows the microscopic images of wound healing for nanofiber groups, including 0% bacterial PHB/Collagen, 25% bacterial PHB/Collagen, and 50% bacterial PHB/Collagen and those loaded with LL37 at the same ratios. When the values were compared, it was observed that wound closure occurred 15–30% faster in the LL37-loaded PHB/Collagen nanofibers (Figure 10).

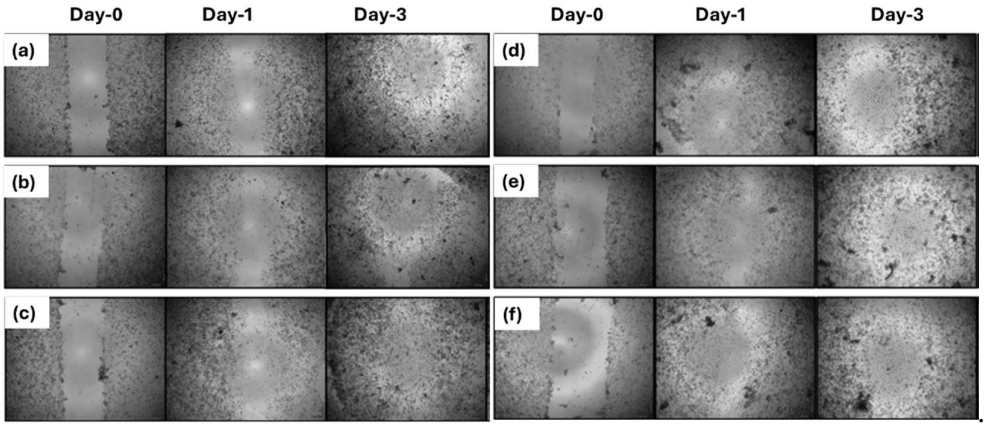

Figure 9. The microscopy views of the scratch assay. After wounding, the NF samples were put on the 2D wounds. After treatment for 1-7 days the cells were monitored by inverted microscope and the wound closure was measured. (a), (b), (c) are NF-1, NF-2, NF-3 and (c), (d), (e) are NF-1/LL37, NF-2/LL37 and NF-3/LL37 respectively. At the 7th day all the scratches were closed.

Parallel to our results, a study by Fahimirad et al. demonstrated that PCL/PVA/CsLL37 and PCL/PVA/CsVEGF scaffolds showed superior wound healing performance compared to PCL/PVA groups, highlighting the wound healing potential of the LL37 AMP [16].

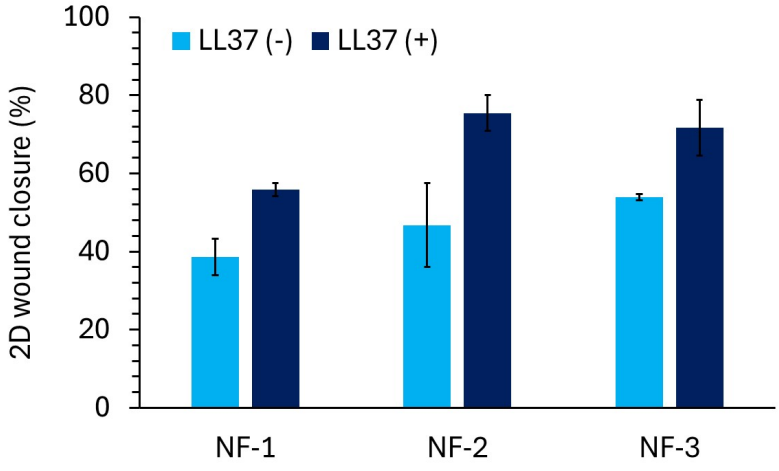

Figure 10. The wound closure % of the NF mat samples, measured by the distance of the closed scratch.

3.6. Antibacterial Activity of Nanofiber Mats

Antibacterial susceptibility tests are performed to determine the in vitro activity of an antimicrobial agent against a specific bacterial strain. Staphylococcus aureus and Escherichia coli were used as representative strains of common wound-associated bacterial infections [17]. Bacterial infections can lead to inflammation, increase exudate production, and negatively impact the wound

 doi:10.20944/preprints202508.0224.v1

healing process. Therefore, it is crucial for an ideal wound dressing to possess antimicrobial properties [18]. Previous studies have demonstrated that LL37 effectively inhibits and disrupts bacterial biofilms by forming ion channels and shows a strong binding affinity to lipopolysaccharides (LPS) present on bacterial membranes, thereby neutralizing bacteria and exhibiting potent antibacterial activity [19]. Similar to LL37's antimicrobial mechanism, PL/LL37 has also been shown to rapidly exert bactericidal activity by forming ion channels in microbial cell membranes and binding to bacterial membrane endotoxins [20]. After treatment with NF/LL37 mats, the viability of S. aureus and E. coli was calculated as a percentage. The viability of S. aureus was reduced by 20–25%, while the viability of E. coli decreased by approximately 80–85% by the 5.57 μM LL37 on the fiber discs (Figure 11). These results indicate that E. coli was more resistant to the LL37 antimicrobial peptide. In a study conducted by Wang and colleagues, LL37 exhibited a stronger inhibitory effect against S. aureus compared to E. coli. The minimum bactericidal concentration (MBC) required to inhibit S. aureus was 4 μM, whereas a higher MBC of 32 μmol/L was required for LL37 to exert bactericidal activity against E. coli [21]. Accordingly, the LL37-loaded PHB/Collagen nanofibers were proven to exhibit antibacterial activity.

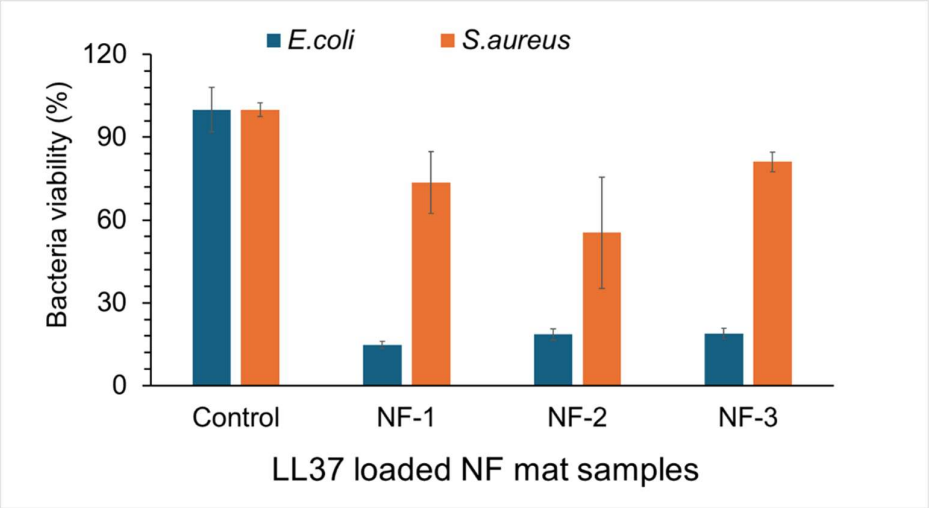

Figure 11. *E. coli* and *S. aureus* viability when treated with NF/LL37 mats.

4. Conclusions

In this study, biocompatible and antibacterial PHB/Collagen nanofiber wound dressing mats loaded with the LL37 peptide were developed via electrospinning. The feasibility of incorporating bacterial PHB (extracted from *Cereibacter sphaeroides*) alongside commercial PHB and marine collagen into stable nanofiber structures with varying bacterial PHB ratios were demonstrated. *In vitro* assessments revealed that the nanofibers were biocompatible with both fibroblast and keratinocyte cells, exhibiting no cytotoxic effects and feasibility as scaffold for cell attachment. In addition, the nanofibers demonstrated inherent antibacterial activity against *Staphylococcus aureus* and *Escherichia coli*. LL37-loaded nanofibers exhibited enhanced wound-healing effects. These results underscore the promising biomedical potential of bacterial PHB in conjunction with collagen and antimicrobial peptides for advanced wound care applications. Future studies may support the in vitro findings with 3D tissue models or in vivo experiments.

Author Contributions: Conceptualization, G.K. , M.D.K., K.Ç.; methodology, B.N.S.T. and S.K.; validation, G.K.; investigation, B.N.S.T.; resources, G.K., M.D.K.; data curation, M.D.K., S.K., K.Ç.; writing—original draft, M.D.K., B.N.S.T.; writing—review and editing, G.K., K.Ç., S.K.; visualization, B.N.S.T.; supervision, G.K.; project administration, M.D.K., G.K., All authors have read and agreed to the published version of the manuscript.

Funding: Horizon Europe, CSA-Twinning REGENEU project. No. 101079123.

 doi:10.20944/preprints202508.0224.v1

Institutional Review Board Statement: Not applicable.

Data Availability Statement: The original contributions presented in this study are included in the article/supplementary material. Further inquiries can be directed to the corresponding author(s).

Acknowledgments: Necmettin Erbakan University BAP-24YL15002 project is acknowledged by the authors.

Conflicts of Interest: The authors declare no conflict of interest.

References

1. J. C. C. Yeo, J. K. Muiruri, W. Thitsartarn, Z. Li, and C. He, "Recent advances in the development of biodegradable PHB-based toughening materials: Approaches, advantages and applications", *Materials Science and Engineering: C*, 92, 1092-1116, 2018, doi: 10.1016/j.msec.2017.11.006.
2. P. Zarrintaj *et al.*, "Biopolymer-based composites for tissue engineering applications: A basis for future opportunities", *Composites Part B: Engineering*, 258, 110701, 2023, doi: 10.1016/j.compositesb.2023.110701.
3. L. J. Borda, F. E. Macquhae, and R. S. Kirsner, "Wound Dressings: A Comprehensive Review", *Curr Derm Rep*, 5, 4, 287-297, 2016, doi: 10.1007/s13671-016-0162-5.
4. P. Martin and R. Nunan, "Cellular and molecular mechanisms of repair in acute and chronic wound healing", *British Journal of Dermatology*, 173, 2, 370-378, 2015, doi: 10.1111/bjd.13954.
5. Y.-H. Wei, W.-C. Chen, H.-S. Wu, and O.-M. Janarthanan, "Biodegradable and Biocompatible Biomaterial, Polyhydroxybutyrate, Produced by an Indigenous Vibrio sp. BM-1 Isolated from Marine Environment", *Marine Drugs*, 9, 4, 2011, doi: 10.3390/md9040615.
6. Roohi, M. R. Zaheer, and M. Kuddus, "PHB (poly-β-hydroxybutyrate) and its enzymatic degradation", *Polymers for Advanced Technologies*, 29, 1, 30-40, 2018, doi: 10.1002/pat.4126.
7. X. Ma *et al.*, "A Review of Antimicrobial Peptides: Structure, Mechanism of Action, and Molecular Optimization Strategies", *Fermentation*, 10, 11, 2024, doi: 10.3390/fermentation10110540.
8. R. Ramos *et al.*, "Wound healing activity of the human antimicrobial peptide LL37", *Peptides*, 32, 7, 1469-1476, 2011, doi: 10.1016/j.peptides.2011.06.005.
9. L. Salvatore *et al.*, "Potential of Electrospun Poly(3-hydroxybutyrate)/Collagen Blends for Tissue Engineering Applications", *Journal of Healthcare Engineering*, 2018, 1, 6573947, 2018, doi: 10.1155/2018/6573947.
10. M. P. Prabhakaran, E. Vatankhah, and S. Ramakrishna, "Electrospun aligned PHBV/collagen nanofibers as substrates for nerve tissue engineering", *Biotechnology and Bioengineering*, 110, 10, 2775-2784, 2013, doi: 10.1002/bit.24937.
11. M. Amir *et al.*, "Polyhydroxybutyrate (PHB) bioplastic characterization from the isolate *Pseudomonas stutzeri* PSB1 synthesized using potato peel feedstock to combat solid waste management", *Biocatalysis and Agricultural Biotechnology*, 57, 103097, 2024, doi: 10.1016/j.bcab.2024.103097.
12. F. Bayram Sarıipek, "Biopolymeric nanofibrous scaffolds of poly(3-hydroxybuthyrate)/chitosan loaded with biogenic silver nanoparticle synthesized using curcumin and their antibacterial activities", *International Journal of Biological Macromolecules*, 256, 128330, 2024, doi: 10.1016/j.ijbiomac.2023.128330.
13. S. Naderi Gharahgheshlagh *et al.*, "Fabricating modified cotton wound dressing via exopolysaccharide-incorporated marine collagen nanofibers", *Materials Today Communications*, 39, 108706, 2024, doi: 10.1016/j.mtcomm.2024.108706.
14. C. Li, L. Du, Y. Xiao, L. Fan, Q. Li, and C. Y. Cao, "Multi-active phlorotannins boost antimicrobial peptide LL-37 to promote periodontal tissue regeneration in diabetic periodontitis", *Materials Today Bio*, 31, 101535, 2025, doi: 10.1016/j.mtbio.2025.101535.
15. M. Mohammadalipour, T. Behzad, S. Karbasi, M. Babaei Khorzoghi, and Z. Mohammadalipour, "Osteogenic potential of PHB-lignin/cellulose nanofiber electrospun scaffold as a novel bone regeneration construct", *International Journal of Biological Macromolecules*, 250, 126076, 2023, doi: 10.1016/j.ijbiomac.2023.126076.
16. S. Fahimirad, M. Khaki, E. Ghaznavi-Rad, and H. Abtahi, "Investigation of a novel bilayered PCL/PVA electrospun nanofiber incorporated Chitosan-LL37 and Chitosan-VEGF nanoparticles as an advanced

 doi:10.20944/preprints202508.0224.v1

antibacterial cell growth-promoting wound dressing", *International Journal of Pharmaceutics*, 661, 124341, 2024, doi: 10.1016/j.ijpharm.2024.124341.

17. Z. Xu *et al.*, "Fighting bacteria with bacteria: A biocompatible living hydrogel patch for combating bacterial infections and promoting wound healing", *Acta Biomaterialia*, 181, 176-187, 2024, doi: 10.1016/j.actbio.2024.04.047.
18. L. Long *et al.*, "Injectable multifunctional hyaluronic acid/methylcellulose hydrogels for chronic wounds repairing", *Carbohydrate Polymers*, 289, 119456, 2022, doi: 10.1016/j.carbpol.2022.119456.
19. B. Bechinger and S.-U. Gorr, "Antimicrobial Peptides: Mechanisms of Action and Resistance", *J Dent Res*, 96, 3, 254-260, 2017, doi: 10.1177/0022034516679973.
20. Z. Liu *et al.*, "Thermal-responsive microgels incorporated PVA composite hydrogels: Integration of two-stage drug release and enhanced self-healing ability for chronic wound treatment", *Chemical Engineering Journal*, 506, 159813, 2025, doi: 10.1016/j.cej.2025.159813.
21. Z. Wang *et al.*, "Thermosensitive-based synergistic antibacterial effects of novel LL37@ZPF-2 loaded poloxamer hydrogel for infected skin wound healing", *International Journal of Pharmaceutics*, 670, 125210, 2025, doi: 10.1016/j.ijpharm.2025.125210.